Composition dependence of interband transition intensities in GaPN, GaAsN, and GaPAs alloys

L. Bellaiche, Su-Huai Wei, and Alex Zunger
National Renewable Energy Laboratory, Golden, Colorado 80401
~Received 10 April 1997!

Using large ~512-atom! pseudopotential supercell calculations, we have investigated the composition dependence of the momentum matrix element $M_{v,c}$ for transitions between the valence-band maximum and the conduction-band minimum of three semiconductor alloys: $GaP_{1-x}N_x$ and $GaAs_{1-x}N_x$, exhibiting large chemical and size differences between their alloyed elements, and $GaP_{1-x}As_x$, which is a weakly perturbed alloy. In the composition ranges where these alloys have a direct band gap, we find that ~i! in $GaP_{1-x}As_x$, $M_{v,c}$ is large ~like the virtual-crystal value! and nearly composition independent; ~ii! in $GaAs_{1-x}N_x$, $M_{v,c}$ is strongly composition dependent: large for small x and small for large x; and ~iii! in $GaP_{1-x}N_x$

in the parent system is of X_{1c} symmetry, the transition to the Γ_v-type valence-band maximum ~VBM! is dipole forbidden. But in the alloy supercell, the CBM could have a Γ_{1c} component so the transition to the VBM can be partially allowed. Such mixing does not exist in the pure parent solids.

Sublattice localization and interband mixing could alter the nature of alloy wave functions relative to the constituents. This could change the interband transition intensities relative to the constituents, leading to a ''bowing'' of the photoluminescence ~PL! intensity.

Previous theoretical and experimental studies of the composition dependence of interband transition intensities are scant. In their supercell tight-binding calculation, Koiller and Capaz[11]

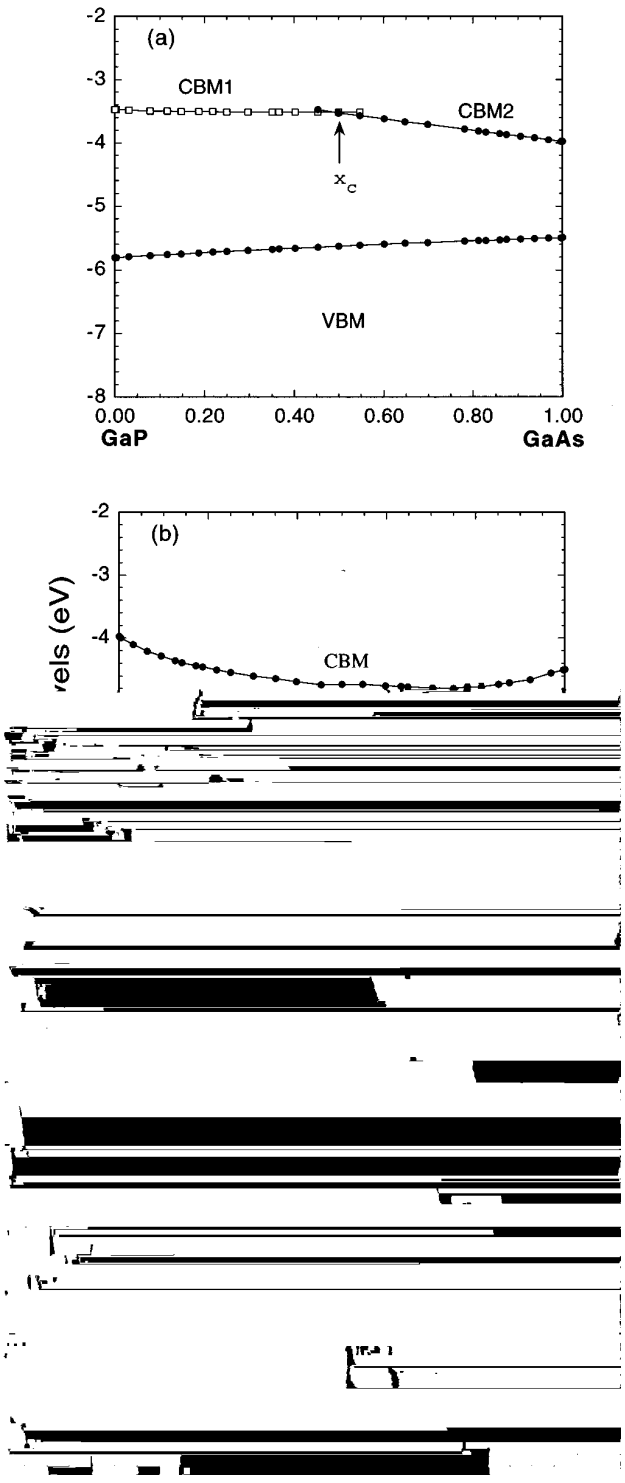

FIG. 1. Composition dependence of the near-edge energy levels of the 512-atom supercell of ~a! $GaP_{1-x}As_x$, ~b! $GaAs_{1-x}N_x$, and ~c! $GaP_{1-x}N_x$ as obtained from atomically relaxed empirical pseudopotential calculations using Vegard's rule for the lattice constant. The valence-band energy is taken as an average over the top three crystal-field split components. Analysis of the wave functions shows that, in GaPAs and GaPN, the CBM reverts from a mostly X_{1c} character ~CBM1! to another state ~CBM2! that has some G_{1c} character. The transition point is $x_c \approx 0.03$ in $GaP_{1-x}N_x$ and $x_c \approx 0.50$ in $GaP_{1-x}As_x$. The bars denote the statistical fluctuations for different, randomly selected configurations, while the arrows emphasize the deep-gap level of GaN:As and GaN:P.

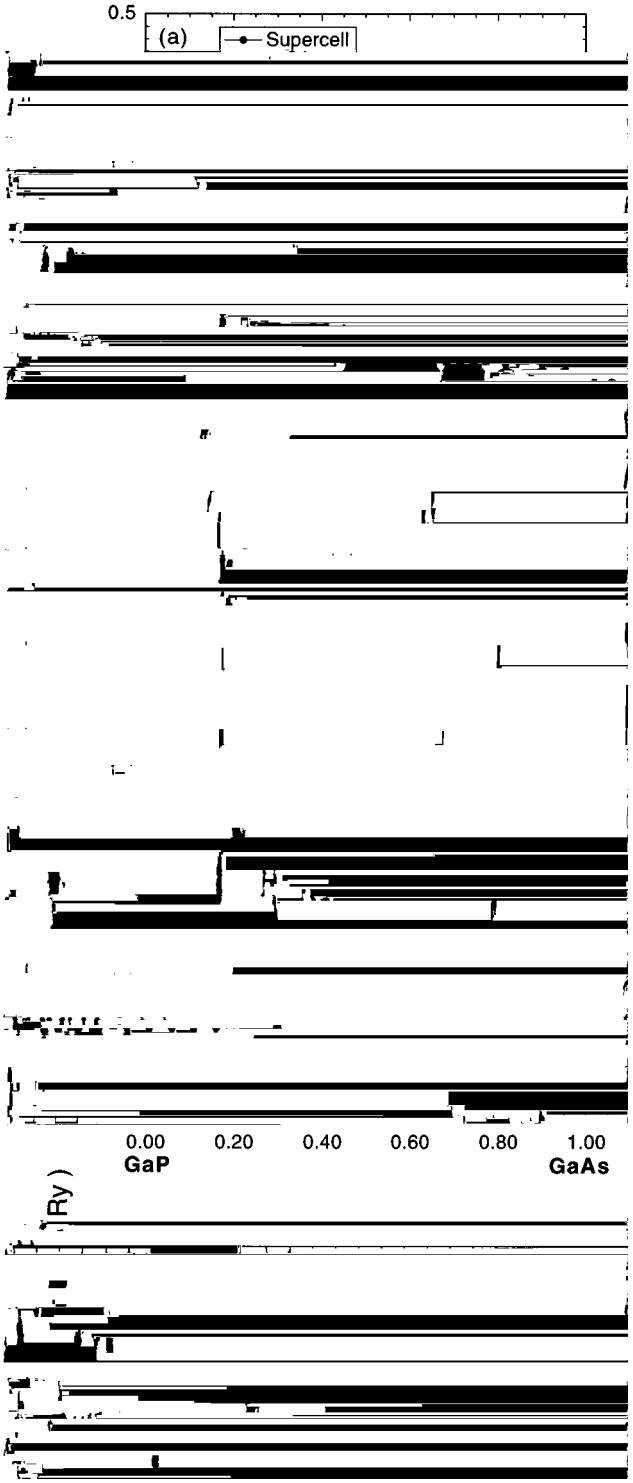

FIG. 2. Square of the momentum matrix element @Eq. ~2!# for the VBM-CBM transition from the supercell ~solid dots! and the unrelaxed VCA ~open squares! calculations in ~a! $GaP_{1-x}As_x$, ~b! $GaAs_{1-x}N_x$, and ~c! $GaP_{1-x}N_x$. The arrows in ~c! point to the composition x_c of the X_{1c}/G_{1c} transition in $GaP_{1-x}N_x$. The bars denote the statistical fluctuations for different, randomly selected configurations.

as well as to other calculations. Due to the large lattice mismatch between GaAs or GaP and GaN, the pseudopotentials were fitted using a composition-dependent kinetic-energy cutoff $G^2_{\max}$ in order to keep the same number of plane waves

per zinc-blende cell for all the compositions ~i.e., volumes!. This kinetic-energy cutoff $G^2_{\max}$ is 5 Ry for GaAs and GaP and 7.87 Ry for GaN, corresponding, in all cases, including our supercell calculations, to 59 plane waves at G per two-atom zinc-blende cell. Since we used *screened* pseudopotentials, our eigenvalues are ''absolute,'' so we can plot separately VBM and CBM energies versus composition. Indeed, superlattice calculations show that the band offsets are the difference between eigenvalues of the constituents.

To calculate near-gap energy levels of large supercells, we use the ''folded spectrum method'':[29] this is a linear-in-size @$O(N)$# method, producing single-particle eigensolutions in a given energy window without having to obtain ~and orthogonalize to! lower eigensolutions. At each composition, results are averaged over a few randomly selected configurations.

Finally, the square of the momentum matrix element is calculated in reciprocal-space from

$$M_{v,c}(\mathbf{K}) = \langle \psi_v(\mathbf{K},\mathbf{r}) | \mathbf{p} | \psi_c(\mathbf{K},\mathbf{r}) \rangle^2 = \left| \sum_{\mathbf{G}} \mathbf{G} C^*_v(\mathbf{K},\mathbf{G}) C_c(\mathbf{K},\mathbf{G}) \right|^2, \quad (2)$$

where the sum runs over the vectors of the reciprocal space and $C_v(\mathbf{K},\mathbf{G})$ and $C_c(\mathbf{K},\mathbf{G})$ are the coefficients of the plane-wave expansion.

III. RESULTS

Figure 1 depicts the composition dependence of the VBM and the CBM energies in $GaP_{1-x}As_x$ @Fig. 1~a!#, $GaAs_{1-x}N_x$ @Fig. 1~b!#, and $GaP_{1-x}N_x$ @Fig. 1~c!#. We see significant differences in the behavior of the two kinds of alloys: The weakly interacting $GaP_{1-x}As_x$ system ~Table I! has much smaller bowing compared to the strongly interacting $GaAs_{1-x}N_x$ and GaP_{1-x}

sponding wave functions via Eq. ~1! shows that in $GaP_{1-x}As_x$ the CBM ~denoted CBM1 in Fig. 1! has mostly X_{1c} symmetry up to x_c . 0.50, at which point it reverts to a state ~denoted CBM2 in Fig. 1! that has mostly Γ_{1c} symmetry. The calculated crossover composition is in good agreement with the experimental results[30–33] of $x_c = 0.51-0.55$. For $GaP_{1-x}N_x$, we predict a crossover composition $x_c = 0.03$ between the conduction states CBM1 ~mostly X_{1c} like! and CBM2 ~contains a Γ_{1c} component as well as many other states!. We are not aware of any direct experimental determination of the crossover composition in $GaP_{1-x}N_x$.

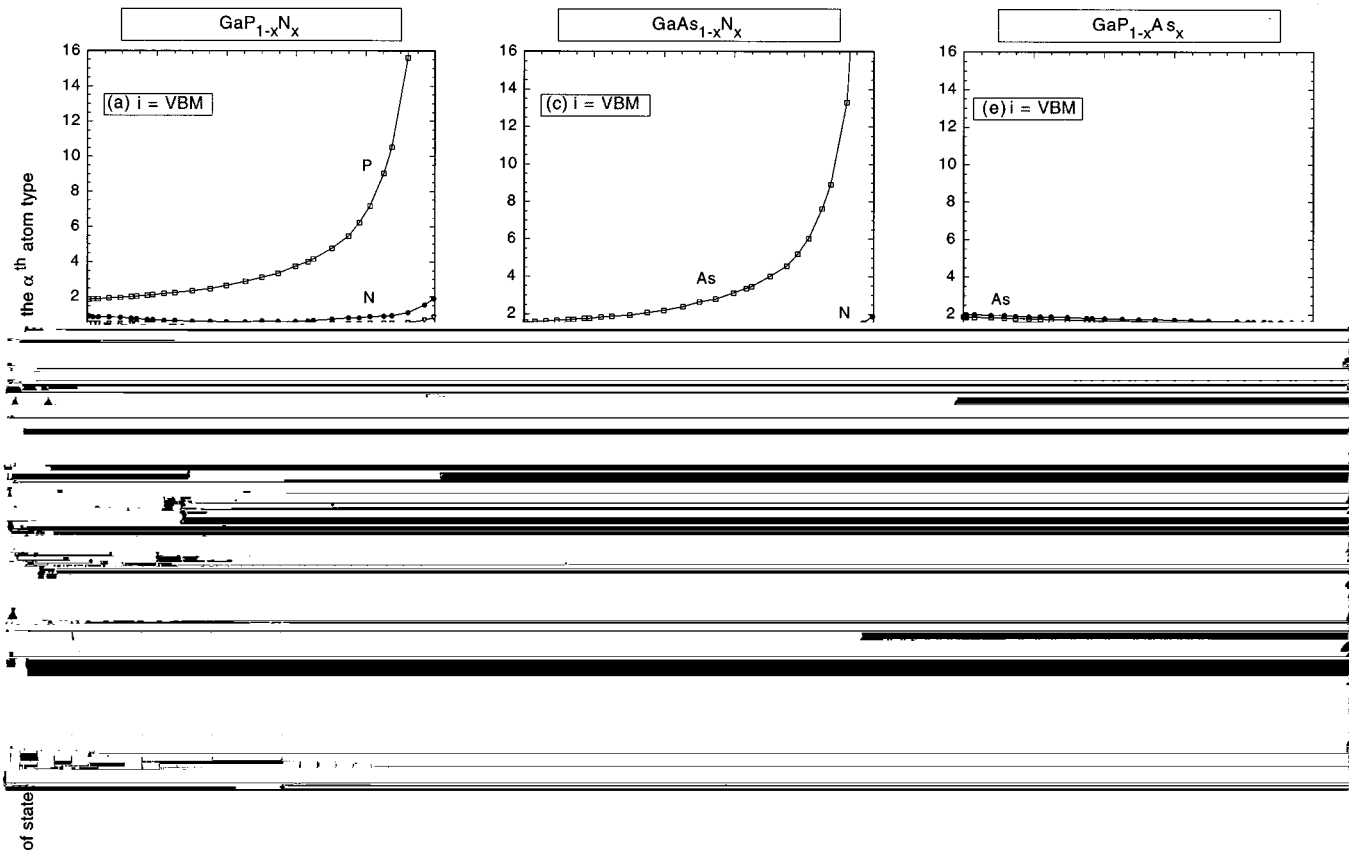

FIG. 4. Average localization parameter $Q_{a,i}$ ~Ref. 14! of the supercell state i 5 VBM and i 5 CBM of atoms of type a 5 (As,P,N,Ga).

by considering Table II: Phosphorus-doped GaN ~denoted GaN:P! is predicted to have a deep, P-localized level @located at 0.61 eV above the VBM of pure GaN ~close to the experimental estimate[36] of 0.57 eV for the wurtzite structure!#, while nitrogen-doped GaP ~denoted GaN:P! has an N-localized level @CBM2 in Fig. 1~c!# ~located at 0.076 eV below the Γ_{1c} state of pure GaP!. Since these impurity states are strongly localized in the real space around the impurity atoms, their wave functions are spread in k space. Due to the wave-function normalization, the projection from the Γ_{15v} or Γ_{1c} VCA state on these impurity states is then reduced by localization. This explains why $B_{\mathrm{VBM},\Gamma_{15v}}$ is small in GaP_eN_{1-e} and why $B_{\mathrm{CBM},\Gamma_{1c}}$ is also small in $GaP_{1-e}N_e$.

The charge localization parameter $Q_{a,i}$ at atom a of the alloy state $c_{i\,5\,\mathrm{VBM}}$ or $c_{i\,5\,\mathrm{CBM}}$ defined in Ref. 14 and displayed in Fig. 4 shows how the VBM wave function becomes more delocalized as the P concentration increases, explaining why $B_{\mathrm{VBM},\Gamma_{15v}}$ approaches continuously its value of 100% at GaP:N. Similarly, the CBM wave function becomes more extended as the N compositions increase @Fig. 4~b!#, explaining why $B_{\mathrm{CBM},\Gamma_{1c}}$ increases progressively until reaching the value of 100% at GaN:P. Since in $GaP_{1-x}N_x$ the VBM and CBM wave-function localizations occur in different composition regions ~high x versus small x, respectively!, the product $B^2_{\mathrm{VBM},\Gamma_{15v}}B^2_{\mathrm{CBM},\Gamma_{1c}}$ is much smaller than 1 for all compositions. This explains why the momentum matrix element of $GaP_{1-x}N_x$ is so weak, in comparison with ''normal'' alloys or with the VCA description of $GaP_{1-x}N_x$. We thus conclude that the weakness of the transition matrix element of $GaP_{1-x}N_x$ reflects wave-function localizations in different composition regions and that these localizations are due to the existences of impurity levels at the dilute impurity limits.

The situation is different in the weakly perturbed $GaP_{1-x}As_x$ system: Since there are no deep impurity levels for GaP:As and GaAs:P,[14] there is no discontinuity of the projections @Fig. 3~g!# at the dilute impurity limits and there is no localization in $GaP_{1-x}As_x$ @Figs. 4~e! and 4~f!#. The projections in this alloy ~Fig. 3! are thus nearly composition independent in the direct-gap region. Consequently, the interband transition probability is large and nearly composition independent in the direct-gap region.

The situation for the $GaAs_{1-x}N_x$ system is intermediate between GaPN and GaPAs: GaN:As has a deep, As-localized impurity level located at 0.75 eV above the VBM of pure GaN,[14] while no impurity state, with Γ_{1c} or Γ_{15v} components, is found for N-doped GaAs.[14] Thus the discontinuity and the weakness of the projections at the dilute impurity limits of this alloy occur only for $B_{\mathrm{VBM},\Gamma_{15v}}$ at x 5 1 2 e @Fig. 3~d!#. The product of the projections is then large for small x and very small for large N compositions where the VBM is strongly localized around the arsenic atoms @see Fig. 3~d!#. Thus this product is strongly composition dependent. We thus conclude that the composition dependence of the transition matrix element of $GaAs_{1-x}N_x$ is due to the existence of an impurity level at ''only'' one impurity limit: GaN:As.

Wave-function localizations and their ensuing effects on

the alloy could be caused by pure chemical differences between the alloyed elements ~as measured, e.g., by the electronegativity difference! or by size differences. To examine which of the two effects is more important, we have selectively eliminated one: We repeated our calculations of the matrix elements in $GaP_{1-x}N_x$ and $GaAs_{1-x}N_x$ *neglecting atomic relaxations* for large x, so the difference between this unrelaxed supercell calculation and the unrelaxed VCA is purely chemical. We found that in the direct-band-gap region ~i! the momentum matrix element is composition independent and nearly equal to the VCA value, ~ii! the band-edge wave functions are extended with large Γ_{15v} or Γ_{1c} characters ~more than 95%!, and ~iii! there is no gap impurity level for GaN:P and GaN:As. Thus we conclude that the strong wave-function localizations and the ensuing weakness of the transition intensities are mostly induced by atomic relaxations for large nitrogen compositions in $GaP_{1-x}N_x$ and $GaAs_{1-x}N_x$.

IV. SUMMARY

We find that in the GaPN alloys ~i! the chemical and particularly the size differences between the two anions lead to localized impurity states in the dilute impurity limits: a P-localized deep impurity state in GaN:P and an N-localized resonant state in GaP:N; ~ii! these states develop into a P-localized VBM in N-rich alloys @Fig. 4~a!# and to an N-localized CBM in P-rich alloys @Fig. 4~b!#; ~iii! these alloy localizations lead to a small projection of the VBM on Γ_{15v} in N-rich alloys and to a small projection of the CBM on Γ_{1c} in P-rich alloys @Fig. 3~a!#; and ~iv! this composition dependence of the projections, when multiplied @$B^2_{\mathrm{VBM},\Gamma_{15v}} B^2_{\mathrm{CBM},\Gamma_{1c}}$; see Fig. 3~b!#, explain the weak and slightly composition-dependent VBM-CBM dipole matrix element in $GaP_{1-x}N_x$ @Fig. 3~c!#. The virtual-crystal approximation forces all anions in $GaP_{1-x}N_x$ to be chemically and, more important, structurally identical. Thus the localization and the composition dependence of the interband matrix element are not allowed in the VCA. In $GaP_{1-x}As_x$ there are no localized states in the impurity limit, so effects ~ii!–~iv! do not exist and the VCA becomes a good approximation for the matrix elements. The situation for $GaAs_{1-x}N_x$ is intermediate between $GaP_{1-x}N_x$ and $GaP_{1-x}As_x$: GaN:As has a deep impurity level, while GaAs:N has no impurity state, with Γ_{1c} or Γ_{15v} components. This leads to a strongly composition dependence of the dipole matrix element @Fig. 3~f!#: $M_{v,c}$ is large for small x and very small for large x.

We wish to emphasize that the calculations here assume a perfectly random alloy, while in reality one might expect important deviations from randomness in the form of clustering[20] or ordering. These may affect optical bowing and momentum matrix elements significantly.

ACKNOWLEDGMENTS

We thank Y. Zhang for useful discussions and A.@666 0 0 6.9

[31] A. Onton and L. M. Foster, J. Appl. Phys. **43**, 5084 ~1972!.
[32] R. J. Nelson, N. Holonyak, and W. O. Groves, Phys. Rev. B **13**, 5415 ~1976!.
[33] H. Mathieu, P. Merle, and E. L. Ameziane, Phys. Rev. B **15**, 2048 ~1977!.
[34] W. Czaja, Festkoerperprobleme **11**, 65 ~1971!.
[35] Y. Zhang, W. Ge, M. D. Sturge, J. Zheng, and B. Wu, Phys. Rev. B **47**, 6330 ~1993!.
[36] J. I. Pankove and J. A. Hutchby, J. Appl. Phys. **47**, 5387 ~1976!.